

AN INTERACTION STUDY BETWEEN PIFAS HANDSET ANTENNA AND A HUMAN HAND-HEAD IN PERSONAL COMMUNICATIONS

A. M. Montaser¹, K. R. Mahmoud^{2,*}, and H. A. Elmikati³

¹Sohag University, Sohag, Egypt

²Department of Electronics and Communications Engineering, Faculty of Engineering, Helwan University, Cairo, Egypt

³Mansoura University, Mansoura 35516, Egypt

Abstract—In this paper, the interaction of a planar inverted-F antennas array, mounted on a mobile handset, with a human hand-head phantom is investigated in the 1.9 GHz band. The hybrid approach involving the particle swarm optimization (PSO) and Nelder-Mead (NM) algorithm is considered to optimize the complex excitations of the adaptive array elements in a mutual coupling environment for different beamforming synthesis. Firstly, the effect of the human hand-head on the handset radiation characteristics is studied. Then, the spatial-peak specific absorption rate (SAR) values of 2- and 4-element PIFA arrays for mobile handset in the vicinity of a human hand-head are evaluated numerically for different scenarios. The antenna is analyzed completely using finite difference time domain (FDTD) method while the interaction is performed using the CST Microwave Studio software.

1. INTRODUCTION

Multiple input and multiple output (MIMO) antenna systems are seen as one of the potential technologies for enhancing performance and capacity of future wireless communication systems [1–5]. They are based on utilizing multiple antennas for both transmission and reception of signals and can allow performance and capacity enhancement without the need for additional power or spectrum [1–3]. Wireless communication devices have also become associated

Received 15 September 2011, Accepted 25 November 2011, Scheduled 1 December 2011

* Corresponding author: Korany Ragab Mahmoud
(KURANY_HAMEDA@h-eng.helwan.edu.eg).

with possible health effects surrounding the exposure of humans to electromagnetic radiation [6, 7]. One of the most widely used parameters for the evaluation of exposure is the specific absorption rate (SAR). Therefore, some regulations and standards have been issued to limit the radiation exposure from the mobile handsets not only to decrease the SAR but also to increase the antenna systems efficiency. The SAR quantifies the power absorbed per unit mass of tissue. This quantity is defined as:

$$SAR = \frac{\sigma}{2\rho} |E_i|^2 \quad (1)$$

where E_i is the max value of the electric field strength in the tissue in V/m, σ is the conductivity of body tissue in S/m, and ρ is the density of body tissue in kg/m³. The SAR limit specified in IEEE C95.1: 2005 has been updated to 2 W/kg over any 10-g of tissue [8]. This new SAR limit specified in IEEE C95.1: 2005 is comparable to the limit specified in the International Commission on Non-Ionizing Radiation Protection (ICNIRP) guidelines [9]. In designing antennas for mobile communications, it is important to investigate the SAR value produced by the radiation from the mobile handsets.

Since the use of adaptive array antennas is one of the most effective ways of increasing the spectral efficiency and improving the communication quality in the mobile communication system, a great deal of attention has turned to how to design antenna arrays on mobile handsets to meet the needs of significantly higher bit-rates for the next-generation wireless communications [10–12]. Many studies on the SAR value of a single antenna for mobile handsets have been carried out in different frequency bands [13–26]. In [27], an investigation of the SAR caused by two-element antenna array at 1.9 GHz has been reported and it was shown that the SAR value reaches a maximum when the phase difference is near 180 degrees and a minimum when the phase difference is approximately 0 degree. The effect of the human head on the accuracy and depth of adaptive nulling for a linear dipole array at 5.0 GHz band is investigated in [28]. This effect is dependent on the separation between the array and the head. A metallic plate is inserted between the array and the head to suppress this effect. In [29], the peak SAR value at 2 GHz and 5 GHz is evaluated numerically as a function of the distance between the array antenna and a spherical head model when the two elements of an antenna array are voltage-fed co-phase or reverse-phase.

A study of how the SAR is affected by different shapes and electrical properties of the human head exposed to a cellular phone have been reported [30]. The results showed that the shape of the human head plays a minor role in calculating the SAR induced in

human head models. In [31], the effect of the human head heterogeneity and shape on the radiation characteristics of dipole antennas has been discussed at 5.0 GHz band. It was found that the input impedance and the radiation pattern of the dipole antenna are not sensitive to the heterogeneity and the shape of the head model.

In [32], the capability of a 5-element monopole array into a handheld device for 4G communication systems in the 5.0 GHz band for beamforming synthesis in a mutual coupling environment is investigated. The interaction of the antenna array, mounted on a mobile handset, with a human head phantom is studied. The spatial-peak specific absorption rate (SAR) values of the smart handset in the vicinity of a spherical phantom of a human head are evaluated numerically as a function of the distance between the handset and the head phantom. It is found that, the resulting SAR values for the smart handset in different scenarios were under the limits set by IEEE C95.1: 2005 or ICNIRP standards.

In this paper, the handset is analyzed completely using CST Microwave Studio, then the CST is linked with the PSO-NM algorithm, Matlab-coded, to optimize the elements weight. Interchanging information between CST Microwave studio and Matlab allows the implementation of mathematical or optimization algorithms and graphical possibilities not included in the Microwave studio environment itself. The approach developed here is very flexible and utilizes the inherent capability of Microwave studio to execute Visual Basic for Applications (VBA) programs. The general idea of this method is that Matlab and CST Microwave studio can interchange information using external text files, which can be read and written by both programs [33]. The PSO-NM algorithm is used to adjust the relative phase shifts and the amplitudes of the excitations of the array elements for beam synthesis in a mutual coupling environment. In particular, we evaluate the potential of a 2- and 4- element PIFA arrays incorporated into a handheld device for beamforming in the 1.9 GHz band. Also, the interaction of the antenna array, mounted on a mobile handset, with a human hand-head phantom is investigated. In addition, the spatial-peak SAR values of 2- and 4-element antenna arrays for mobile handset in the vicinity of a human hand-head are evaluated numerically for different scenarios. The total power delivered to all antenna arrays for all cases is held constant (100 mW).

The organization of the present paper is as follows: In Section 2, a brief introduction to the hybrid particle swarm optimization and nelder mead (PSO-NM) algorithm is presented. In Section 3, handset design and simulation results for two and four elements PIFA array mounted on the mobile handset are discussed. The interaction between the

handset and the human hand-head is investigated in Section 4. Finally, Section 5 presents the conclusions.

2. PARTICLE SWARM OPTIMIZATION — NELDER MEAD (PSO-NM) ALGORITHM

PSO is a population based optimization tool, where the system is initialized with a population of random particles and the algorithm searches for optima by updating generations [34]. Suppose that the search space is D -dimensional. The current position of the i -th particle can be represented by a D -dimensional vector $X_i = (x_{i1}, x_{i2}, \dots, x_{iD})$ and the velocity of this particle is $V_i = (v_{i1}, v_{i2}, \dots, v_{iD})$. The best previously visited position of the i -th particle is represented by $P_i = (p_{i1}, p_{i2}, \dots, p_{iD})$ and the global best position of the swarm found so far is denoted by $P_g = (p_{g1}, p_{g2}, \dots, p_{gD})$. The fitness of each particle can be evaluated through putting its position into a designated objective function. The particle's velocity and its new position are updated as follows:

$$v_{id}^{k+1} = \omega v_{id}^k + c_1 r_1^k (p_{id}^k - x_{id}^k) + c_2 r_2^k (p_{id}^k - x_{id}^k) \quad (2)$$

$$x_{id}^k = x_{id}^k + v_{id}^{k+1} \Delta t \quad (3)$$

where $d \in \{1, 2, \dots, D\}$, $i \in \{1, 2, \dots, N\}$, N is the population size, the superscript k denotes the iteration number, ω is the inertia weight, r_1 and r_2 are two random values in the range $[0, 1]$, c_1 and c_2 are the cognitive and social scaling parameters which are positive constants ($c_1 = 2.8$ and $c_2 = 1.3$). In this paper, the PSO algorithm is employed with a population size of 20 and 50 iterations. For beamforming synthesis, the amplitude was allowed to vary between 1.0 and 3.0 and the phase was allowed to vary between $-\pi$ and π .

A very simple objective function for the antenna array is used for maximizing the output field toward the desired signal at θ_i and minimizing the total output field in the direction of the interfering signals at θ_j .

$$\text{Objective-function} = \sum_{i=1}^N a_i |E(\theta_i)| - \sum_{j=1}^M b_j |E(\theta_j)| \quad (4)$$

where $E(\theta)$ is the total electric field and the constants a_i and b_j are the weights that control the contribution from each term to the overall objective function. The constants N and M represent the number of desired signals and interferers respectively. In our analysis, we take the weights $a_i = 2$ and $b_j = 1$ to give some priority to maximizing the output field toward the desired signal rather than minimizing the output field in the direction of the interfering signals.

Once the global optima using PSO algorithm is completed; the Nelder-Mead (NM) local optimization technique is followed to fine optimize the results. The NM method thus falls in the general class of direct search methods. It is based on the comparison of the function values at the $(D + 1)$ vertices for D -dimensional decision variables. Selection of these points can be prescribed, but random selection allows the potential to fully investigate the merit space [35].

3. HANDSET DESIGN AND SIMULATION RESULTS

The geometry of the PIFAs and printed circuit board (PCB) layout for our prototype are shown in Fig. 1. Fig. 1(a) shows the geometry of the 2-PIFA antenna elements and Fig. 1(b) for the four elements PIFA array. The dimensions of the PCB are $(l = 110 \text{ mm}, w = 50 \text{ mm})$ while the size of the PIFAs are $P_L = 34 \text{ mm}, P_w = 10 \text{ mm}$ with heights of $h = 6 \text{ mm}$ and PIFA separation, $d = 20 \text{ mm}$. The FDTD method written with MATLAB software [36] is used to design a two and four elements PIFA array and the results are compared with that obtained using CST Microwave Studio. The parameters for FDTD computation were set as follows for 2-PIFA array: the domain was $147 \times 100 \times 20$ cells with a cell size of $\Delta x = 0.75 \text{ mm}, \Delta y = 0.5 \text{ mm}, \Delta z = 0.5 \text{ mm}$. While for 4-PIFA elements, the domain was $147 \times 100 \times 40$ cells with the same cell sizes used for 2-PIFA elements. The FDTD lattice needs to be terminated by perfectly matched layer (PML) on all sides; a spatially varying conductivity should be used in order to avoid numerical reflections at the interface of FDTD/PML regions. For two

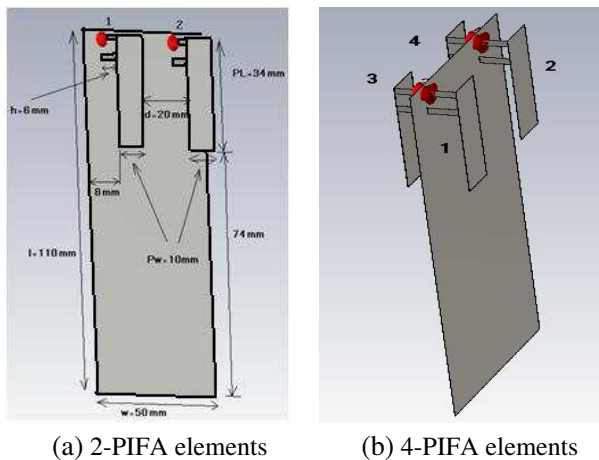


Figure 1. Geometry of the two and four element PIFA array.

antenna structures, the computational domain was terminated with perfectly matched layer (PML) of 8 cells in all directions with a time step of 1.452 ps. For the CST Microwave Studio simulator, which based on the Finite Element Method (FEM), the following settings were used for time domain simulations: the minimum mesh step = 0.535, maximum mesh step = 12.637 and the mesh cells = 22.185 ($N_x = 52$, $N_y = 30$, $N_z = 16$). The mesh line ratio limit was set to 50 with an equilibrate mesh ratio of 1.19. Open add space boundary condition is applied in all directions with thermal boundaries isothermal ($T = \text{constant}$).

The primary difference between the FDTD and the FEM method is that, the FDTD discretize the problem into small rectangular cells, these cells possible allocation of the six electric and magnetic components are located at the edges and on the surfaces of the cell [36]. While in the FEM, the problem space is discretized into small shapes which results in a mesh with grid nodes, the solution can be approximated with a simple function, the so-called shape function, in each element, which acts as a contribution to the approximation of the global solution.

Figures 2(a), (b), (c), (d) show the results comparison between the FDTD method, the EM Simulator of CST Microwave Studio software, and measurement results [27] for S parameters (S_{11} , S_{12} , S_{21} , S_{22}) for two elements PIFA array. In general, good agreement is seen between the computed values and measurements up to the readability of the figures in [27]. There are some differences between the calculated results due to the different applied numerical techniques (FDTD and FEM). Compared to the measured results, the FDTD results are slightly more accurate than the CST MWS results. From Fig. 2, it can be observed that both PIFA antennas achieve S_{11} and S_{22} of less than -10 dB around 1.9 GHz with a mutual coupling less than -9 dB. Although mutual coupling of -9 dB is not insignificant it is generally accepted that envelope signal correlations between the antennas in realistic mobile environments only needs to be less than 0.5 [2, 4, 5]. Using the bound $\rho_e < 25|S_{12}|^2$ (which is valid if the magnitude of the S -parameters satisfy the condition $|S_{11}| + |S_{22}| + |S_{11}||S_{22}| + |S_{12}||S_{21}| < 0.25$ and is also satisfied in our results) it can be shown that $\rho_e < 0.39$ indicating that sufficient diversity would be achieved [2, 4, 5]. Figs. 3(a), (b), (c), (d) show the comparison between the simulated results using the FDTD method and the CST Microwave Studio software for S parameter (S_{11} , S_{21} , S_{31} , S_{41}) for 4-elements PIFA array. It is found that, the 4-PIFA antenna array has a resonance frequency of 1.9 GHz with a return loss less than -11.5 dB with acceptable coupling between antenna elements.

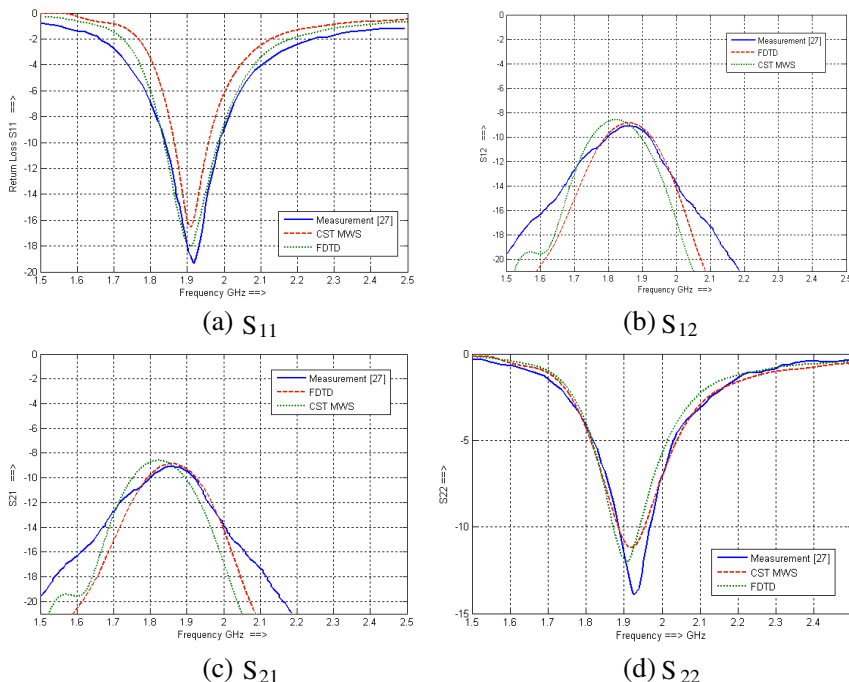


Figure 2. The comparison between simulated results using the FDTD method, CST microwave studio software and measurement results for S parameter (S_{11} , S_{12} , S_{21} , S_{22}) for two elements PIFA array.

The PSO-NM algorithm has been programmed in Matlab in connection with the CST simulator for the calculation of the fitness value of each particle. The process for communicating CST and Matlab is as follows: First, using PSO-NM as it is described in Section 2, the values for the parameters to be optimized are generated using Matlab. These values are saved in a text file. A Visual Basic for Applications macro (VBA) is the most straightforward way to run the CST simulation from Matlab. Second, Matlab calls CST and a VBA macro loads the data from the text file and stores the values in CST variables. Then, a new macro is called for creating the structure of the proposed device according to the values of the variables previously loaded and starts the simulation. When the simulation finishes, the results for radiation pattern will be saved in a new text file and CST is closed. Finally, Matlab reads the radiation pattern results from the file and the fitness function is calculated. This process is repeated for each particle. Fig. 4 shows a flowchart diagram of the main steps to link the Matlab with the CST simulator.

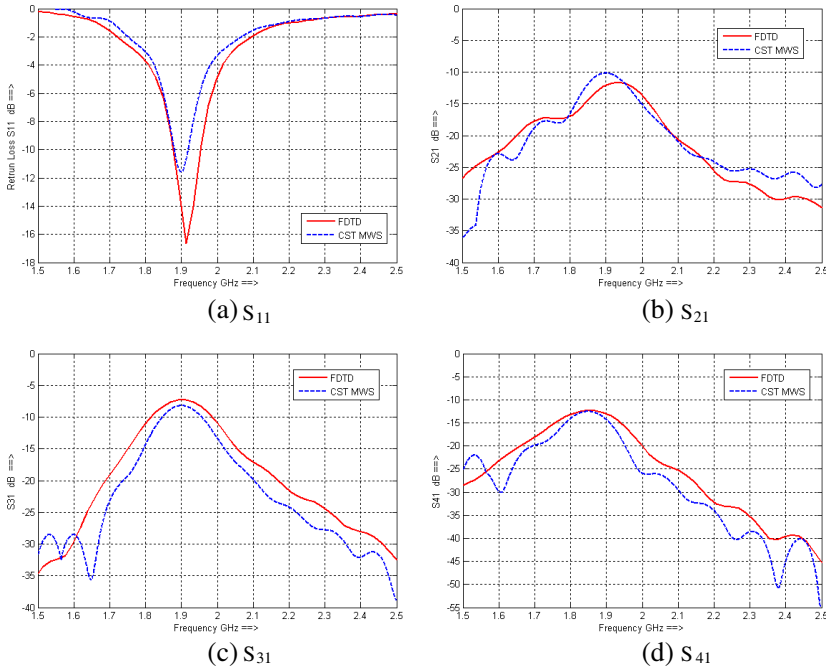


Figure 3. The comparison between simulated with FDTD method, CST Microwave Studio software for S parameter (S_{11} , S_{21} , S_{31} , S_{41}) for four elements PIFA array.

Table 1. Descriptions of the environmental scenarios.

Scenario #1				Scenario #2			
<i>Desired</i>	<i>Interference</i>			<i>Desired</i>	<i>Interference</i>		
0°	90°	180°	270°	30°	90°	180°	270°
Scenario #3				Scenario #4			
<i>Desired</i>	<i>Interference</i>			<i>Desired</i>	<i>Interference</i>		
120°	0°	90°	270°	210°	0°	90°	270°

As an example of adaptive beamforming, four scenarios were considered as shown in Table 1. Fig. 5 shows the capability of the 2-element array geometry to direct the maximum field towards the direction of Signal Of Interest (SOI) while placing deeper nulls towards the angles of Signal Not Of Interest (SNOI) for different scenarios. The required amplitude and phase excitations of each element to obtain

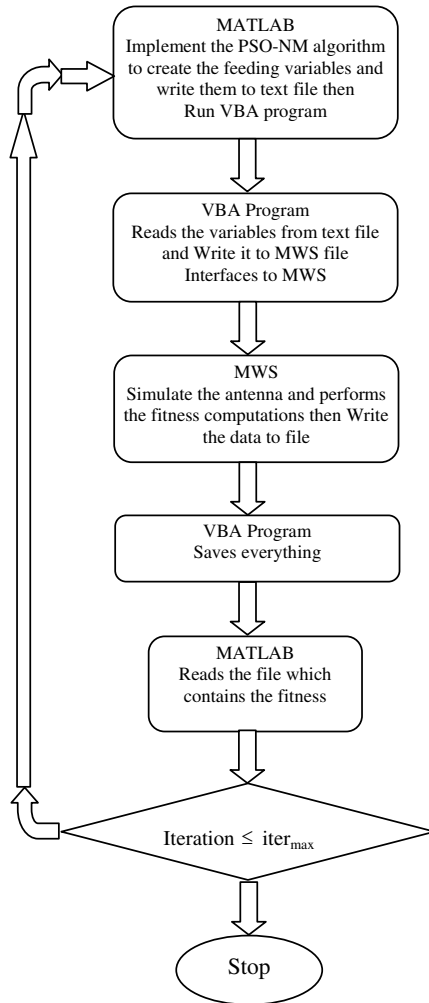


Figure 4. Flowchart showing the main steps to link the Matlab with the CST simulator.

the beam patterns in Fig. 5 are shown in Table 2. It is found that an acceptable gain of 4.12, 3.85, 4.35, and 4.55 dBi are obtained in the direction of SOI for different scenarios 1, 2, 3, and 4 respectively. Similarly, the same scenarios are applied to the 4-elements PIFA array as shown in Fig. 6. The required amplitude and phase excitations of each element to obtain the beam patterns in this figure are shown in Table 3. The calculated gain for different scenarios (1, 2, 3, 4) are

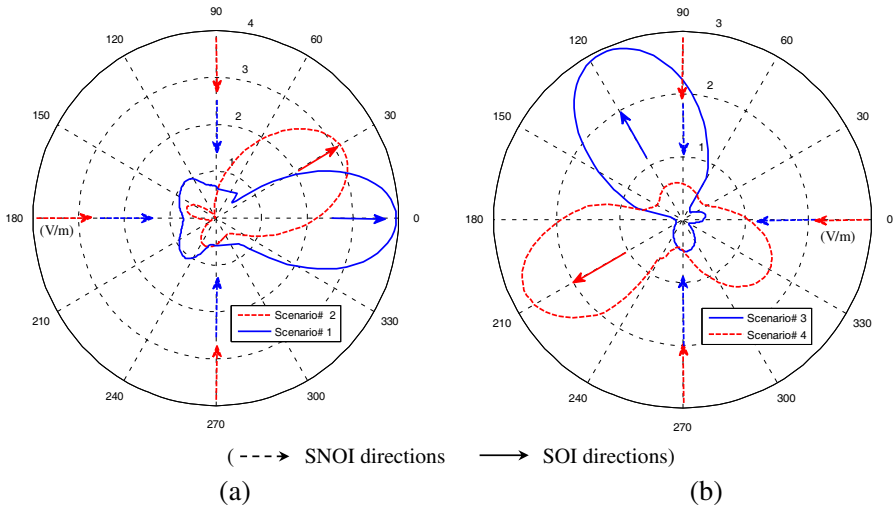


Figure 5. The radiation pattern $|E|$ for the two element PIFA array. (SNOI directions SOI directions).

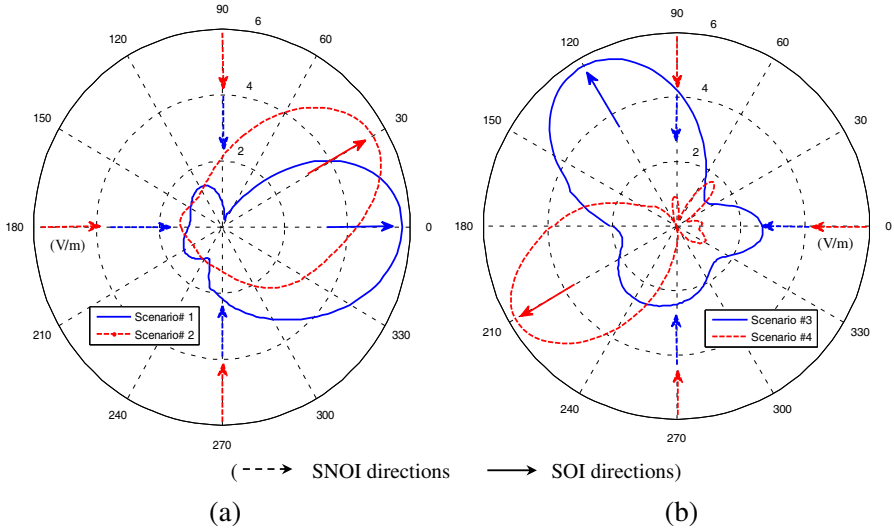


Figure 6. The radiation pattern $|E|$ for the four element PIFA array. (SNOI directions SOI directions).

found to be 4.7, 4.81, 4.67, and 4.46 dBi respectively. It is found that for a uniform feeding PIFA array (scenario # 0) where all elements are excited with the same amplitude and phase ($2, 0^\circ$), the gain of the 4-PIFA elements is slightly higher than that of the 2-PIFA elements by

Table 2. The required amplitude and phase excitations of each element for 2-element PIFA array for different scenarios with the corresponding gain.

<i>Element No.</i>	Scenario #1		Scenario #2	
	<i>amplitude</i>	<i>phase</i>	<i>amplitude</i>	<i>phase</i>
1	2.97	75.728°	2.61	-81.19°
2	2.55	47.33°	2.49	-116.71°
<i>Element No.</i>	Scenario #3		Scenario #4	
	<i>amplitude</i>	<i>phase</i>	<i>amplitude</i>	<i>phase</i>
1	1.73	-73.25°	2.65	-97.44°
2	2.05	-11.13°	1.93	-129.94°

Table 3. The required amplitude and phase excitations of each element for 4-element PIFA array for different scenarios with the corresponding gain.

<i>Element No.</i>	Scenario #1		Scenario #2	
	<i>amplitude</i>	<i>phase</i>	<i>amplitude</i>	<i>phase</i>
1	2.41	68.025°	2.98	94.096°
2	1.72	128.97°	1.97	145.456°
3	1.64	-135.77°	1.76	-139.96°
4	2.72	-8.974°	2.98	-10.981°
<i>Element No.</i>	Scenario #3		Scenario #4	
	<i>amplitude</i>	<i>phase</i>	<i>amplitude</i>	<i>phase</i>
1	2.76	-24.21°	1.72	-40.671°
2	2.44	-23.20°	1.46	-1.996°
3	1.64	5.272°	2.85	95.573°
4	1.23	-156.84°	1.04	-4.568°

0.32 dB. Generally, the obtained gain for different scenarios (1, 2, 3, 4) is found to be higher than that of the uniform feeding case (scenario # 0); due to directing the power to only one direction (Base Station).

4. INTERACTION BETWEEN HANDSET AND HUMAN HAND-HEAD

In this section, the interaction between the mobile handset and the human hand-head has been studied. The described antennas in

Section 3 are now covered with a dielectric material ($\epsilon_r = 2.1$), having external dimensions of $113.6 \times 53.6 \times 9.6$ mm for 2-PIFA antenna elements and $113.6 \times 53.6 \times 15.6$ mm for 4-PIFA case. The SAM phantom head and hand that provided by CST Microwave Studio is used [37]; the tissue that it contained had a relative permittivity and conductivity as shown in Table 4. These tissue-equivalent dielectric parameters were chosen according to [38] for simulating brain tissue at 1.9 GHz. The head phantom was finely meshed to give voxels of 8 mm^3 , corresponding to a sampling mesh of 2 mm along each Cartesian axis. The final number of mesh-cells sums up to be around 11 Million cells. The relative position of the handset relative to human head model is illustrated in Fig. 7. The interaction between the mobile handset and the human hand-head is studied from two viewpoints, the effect of the human hand-head on the handset radiation characteristics in different scenarios and the impact of the handset on SAR.

Firstly, we will study the effect of the human hand-head on the handset radiation characteristics. As shown in Fig. 7, the handset has

Table 4. The conductivity and relative dielectric constant at 1.9 GHz for the head model.

Tissue	Permittivity	Conductivity
Avg. Brain	43.374870	1.203850
Avg. Skull	15.465057	0.456124
Avg. Muscle	54.304787	1.447971
Palm (Skin) Dry	38.714	1.2245

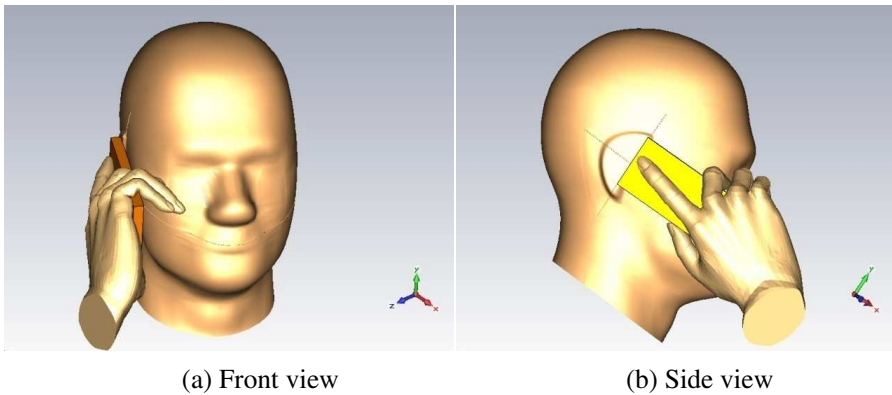
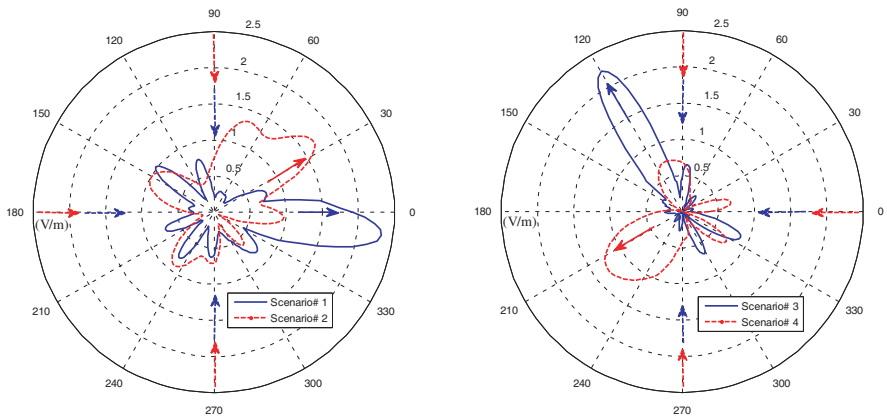
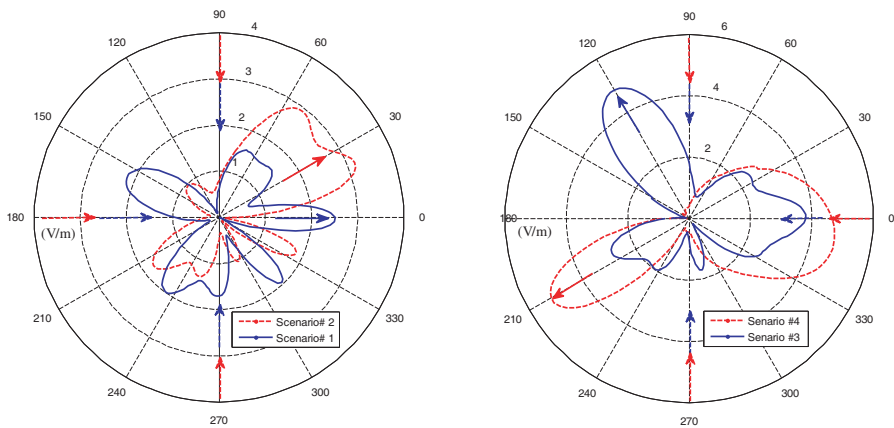


Figure 7. Human hand-head model and handset configuration.

placed in parallel tendency according to the situation palm of the hand to simulate the actual status of the handset user. The distance between the nearest points for palm hand and the human head model is 5 mm. Fig. 8 shows the handset radiation pattern in the presence of the SAM phantom head and hand that provided by CST Microwave Studio for both 2- and 4-PIFA handsets. It is noted that, the radiation pattern is affected by the presence of the human hand-head. Therefore, the beam patterns need to be re-optimized in the presence of the human hand-head.



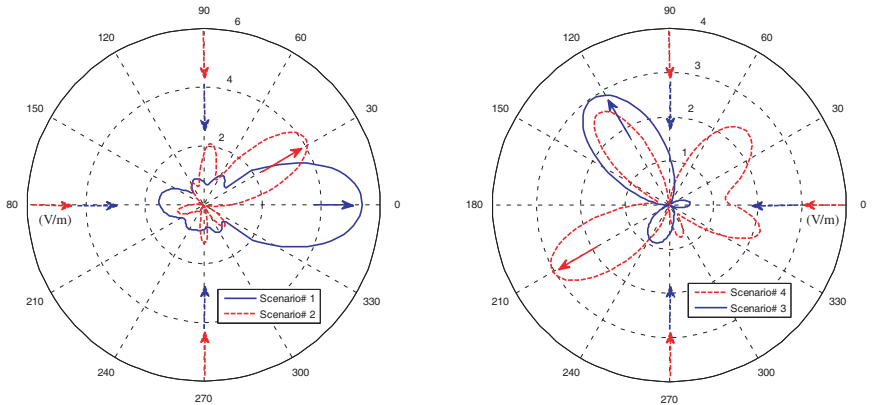
(a) Two elements PIFA array mounted on the mobile handset



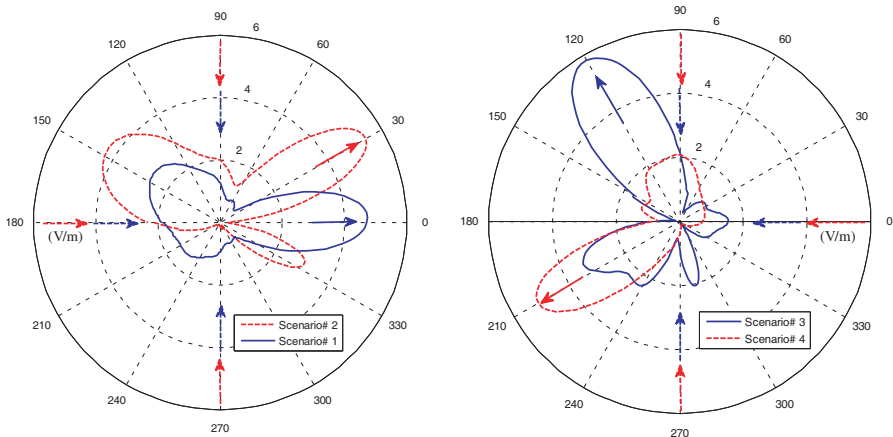
(b) Four elements PIFA array mounted on the mobile handset

Figure 8. The radiation pattern $|E|$ of the handset in the presence of the human hand-head phantom (pre-optimized beam pattern).

Figure 9 shows the re-optimized beam patterns of the handsets in the presence of the SAM phantom human hand-head for scenarios 1, 2, 3 and 4. The figure shows the ability of the design to direct the maximum field towards the direction of SOI while placing deeper nulls towards the angles of SNOI in the presence of the human hand-head for different scenarios. The required amplitude and phase excitations of each element to obtain the beam patterns for two and four elements PIFA array on a handset in this figure are shown in Tables 5 and 6, respectively.



(a) Two elements PIFA array mounted on the mobile handset



(b) Four elements PIFA array mounted on the mobile handset

Figure 9. The radiation pattern $|E|$ of the handset in the presence of the human head phantom (optimized beam pattern).

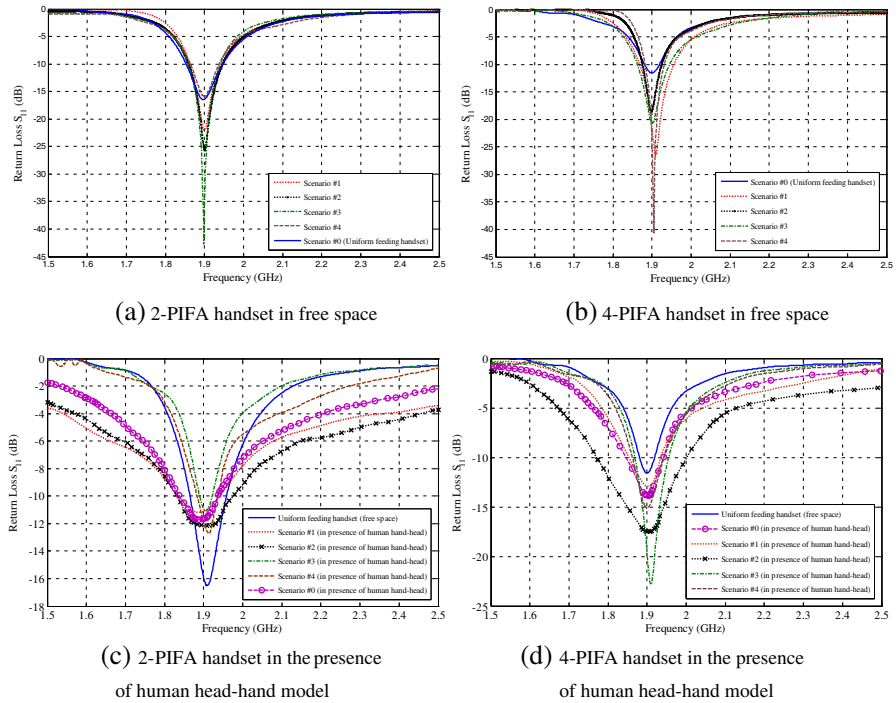


Figure 10. The return loss results comparison of both handsets in free space and in the presence of human head-hand model for different scenarios.

Table 5. The required amplitude and phase excitations of each element for the 2-element PIFA handset in the presence of the SAM phantom human hand-head for different scenarios.

<i>Element No.</i>	Scenario #1		Scenario #2	
	<i>amplitude</i>	<i>phase</i>	<i>amplitude</i>	<i>phase</i>
1	1.43	169.29°	1.02	102.02°
2	2.73	139.69°	2.27	47.383°
<i>Element No.</i>	Scenario #3		Scenario #4	
	<i>amplitude</i>	<i>phase</i>	<i>amplitude</i>	<i>phase</i>
1	1.56	67.32°	1.59	155.20°
2	2.49	103.93°	2.92	75.61°

Figure 10 shows the comparison of the return loss results of both handsets in free space and presence of human hand-head model for different scenarios. It is found that for all scenarios the handsets resonance frequency still around 1.9 GHz but with different values of S_{11} . The different values of S_{11} from scenario to another are related to the change in the feeding weights for each scenario.

Nowadays, all newly proposed handset antennas consider the SAR as an important design specification that they must meet. Therefore,

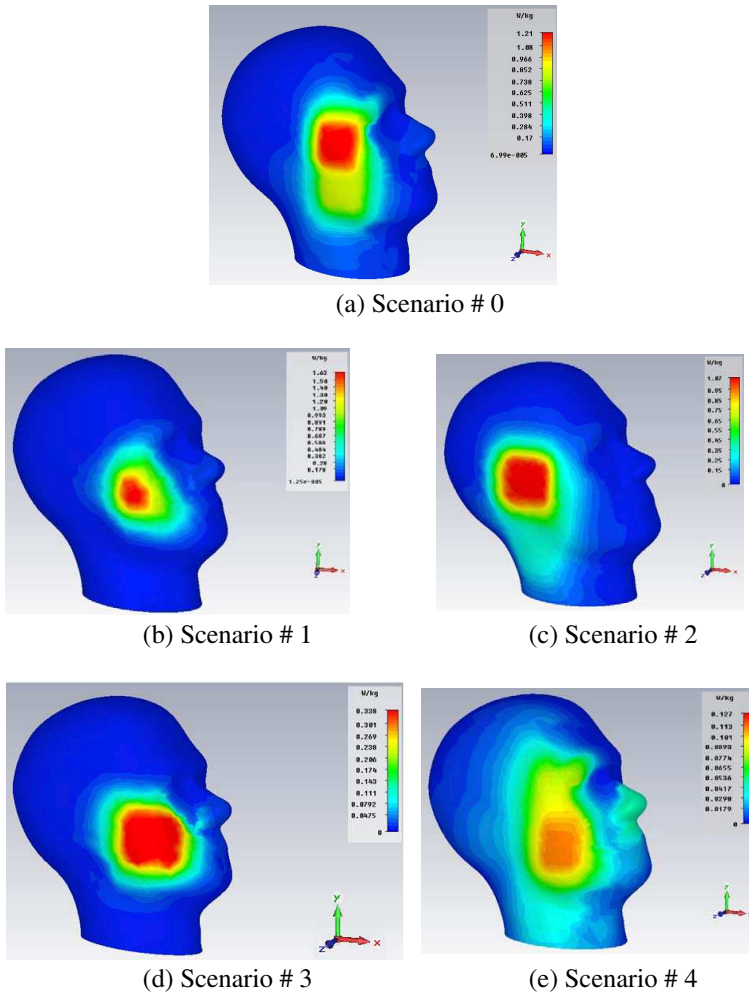


Figure 11. SAR in full human head phantom for different scenarios.

Table 6. The required amplitude and phase excitations of each element for the 4-element PIFA handset in the presence of the SAM phantom human hand-head for different scenarios.

<i>Element No.</i>	Scenario #1		Scenario #2	
	<i>amplitude</i>	<i>phase</i>	<i>amplitude</i>	<i>phase</i>
1	2.96	-47.34°	1.97	-59.85°
2	2.17	-17.29°	2.97	-27.05°
3	2.38	63.87°	1.53	132.54°
4	1.03	-20.13°	1.14	-16.76°
<i>Element No.</i>	Scenario #3		Scenario #4	
	<i>amplitude</i>	<i>phase</i>	<i>amplitude</i>	<i>phase</i>
1	1.75	-2.108°	2.03	22.103°
2	1.37	134.29°	1.39	140.754°
3	2.01	-75.175°	1.48	-14.408°
4	2.18	10.045°	2.94	-101.61°

Table 7. Comparison between spatial-peak SAR over 10-g, gain and S_{11} of two and four elements PIFA handset in the presence of human hand-head for different scenarios.

		SAR (W/kg)	Gain (dBi)	(S_{11})_{f=1.9 GHz} (dB)
2-PIFA Handset Scenarios	Scenario # 0	1.087	3.31	-11.7
	Scenario # 1	1.167	3.98	-11.12
	Scenario # 2	0.852	3.7	-12.14
	Scenario # 3	0.0371	4.31	-10.95
	Scenario # 4	0.0778	4.17	-11.87
4-PIFA Handset Scenarios	Scenario # 0	1.21	4.53	-13.82
	Scenario # 1	1.63	5.21	-12.89
	Scenario # 2	1.067	4.93	-17.53
	Scenario # 3	0.338	4.86	-19.77
	Scenario # 4	0.127	4.75	-15.11

in this section we will study the impact of the handset on SAR. Fig. 11 shows the SAR human head phantom for 4-PIFA handset in different scenarios including the uniform feeding case (scenario # 0). It is noted that, when the PIFA array elements are fed with different voltage values to achieve certain scenario, the spatial-peak

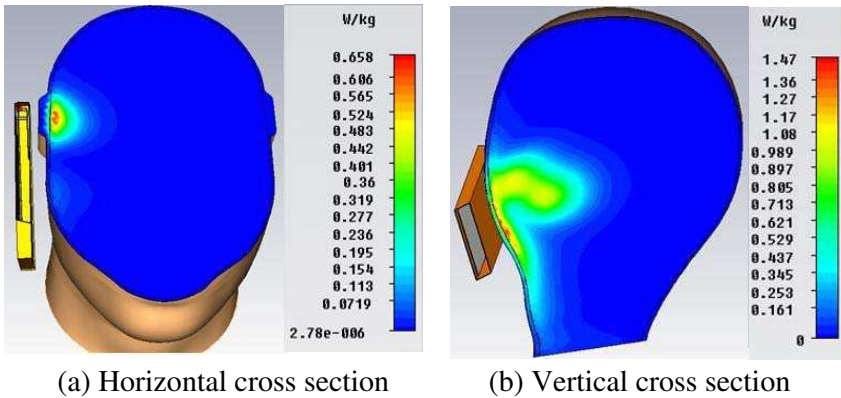


Figure 12. Horizontal and vertical cross section in human head phantom for scenario # 1 (worst SAR).

SAR is affected significantly. As shown in Fig. 11, the position of the spatial-peak SAR over 10-g on the human head is changed from scenario to another in addition to the effective field size. It is found that the highest spatial-peak SAR over 10-g is for scenario #1 ($\text{SAR} = 1.63 \text{ W/kg}$) but for other scenarios such as scenario # 4 the SAR is decreased to 0.127 W/kg compared to 1.21 W/kg for a uniform feeding case (scenario # 0). Fig. 12 shows the horizontal and vertical cross section human head phantom for scenario # 1 which corresponding to the worst case to illustrate the penetration depth of field inside the human head. It is found that, the highest SAR value is obtained in the region of the skin near the handset. In addition, some other issues should be noted as well, as suggested by a comparison of the SARs induced in the realistic human-head model for the homogeneous and the inhomogeneous cases [30]. It is found that the constitutive parameters of a human head significantly affect the result of the SAR induced in homogeneous or inhomogeneous head models where the local maximum SAR induced in the homogeneous human-head model is larger than that induced in the inhomogeneous human head model. That means that the simulated SAR values in this paper conservative estimate for the homogeneous human head model, however, these values of SAR for the smart handsets in different scenarios are under the limits set by IEEE C95.1: 2005 or ICNIRP standards with acceptable gain values. Table 7 shows the spatial-peak SAR over 10-g for two and four elements PIFA array on a handset in addition to handset antenna gain and return loss for all scenarios in the presence of human hand-head at 1.9 GHz.

5. CONCLUSION

In this paper, we investigated the capability of a 2- and 4-elements PIFA array into a handheld device for communication systems in the 1.9 GHz band for beamforming synthesis in a mutual coupling environment. The PSO-NM algorithm is used to optimize the complex excitations of the adaptive arrays elements for beamforming. Also, the interaction of the antenna array, mounted on a mobile handset, with a human hand-head phantom is investigated. It is found that, the radiation pattern is affected by the presence of the human hand-head. Therefore the beam patterns should be optimized in the presence of the human hand-head. The spatial-peak SAR values of the smart handset in the vicinity of the SAM phantom head and hand is also considered for different scenarios. The numerical simulation results demonstrated that the smart handset can work under SAR guidelines limitations.

ACKNOWLEDGMENT

We would like to acknowledge the Electronics Research Institute (ERI), Microstrip Department for the support, encouragement, help and cooperation during simulation process of this research.

REFERENCES

1. Lozano, A., F. R. Farrokhi, and R. A. Valenzuela, "Lifting the limits on high-speed wireless data access using antenna arrays," *IEEE Commun. Mag.*, Vol. 39, 156–162, Sep. 2001.
2. Winters, J. H., "Smart antennas for wireless systems," *IEEE Personal Commun. Mag.*, Vol. 5, 23–27, Feb. 1998.
3. Murch, R. D. and K. B. Letaief, "Antenna systems for broadband wireless access," *IEEE Commun. Mag.*, Vol. 40, 76–83, Apr. 2002.
4. Ko, C. K. and R. D. Murch, "Compact integrated diversity antenna," *IEEE Trans. Antenna Propagat.*, Vol. 49, 954–960, Jun. 2001.
5. Vaughan, R. G. and J. B. Andersen, "Antenna diversity in mobile communications," *IEEE Trans. Veh. Technol.*, Vol. 36, No. 4, 149–172, Nov. 1987.
6. Rosen, A. and A. Vander Vorst, "Special issue on medical application and biological effects of RF/microwaves," *IEEE Trans. Microwave Theory Tech.*, Part II, Vol. 44, Oct. 1996.

7. Rosen, A., A. Vander Vorst, and Y. Kotsuka, "Special issue pm medical applications and biological effects of RF/microwaves," *IEEE Trans. Microwave Theory Tech.*, Part II, Vol. 48, Nov. 2000.
8. IEEE C95.1:2005, "Safety levels with respect to human exposure to radio frequency electromagnetic fields, 3 kHz to 300 GHz," IEEE standard, 2005.
9. ICNIRP Guidelines, "Guidelines for limiting exposure to time-varying electric, magnetic, and electromagnetic fields (up to 300 GHz)," *Health Phys.*, Vol. 74, No. 4, 1998.
10. Dietrich, Jr., C. B., W. L. Stutzman, B. Kim, and K. Dietze, "Smart antennas in wireless communications: Base-station diversity and handset beamforming," *IEEE Antennas and Propagation Magazine*, Vol. 42, No. 5, 142–151, Oct. 2000.
11. Denidni, T. A., D. McNeil, and G. Y. Delisle, "Experimental investigations of a new adaptive dual-antenna array for handset applications," *IEEE Trans. Veh. Technol.*, Vol. 52, No. 6, 1417–1423, Nov. 2003.
12. Yuan, Q., Q. Chen, and K. Sawaya, "Performance of adaptive array antenna with arbitrary geometry in the presence of mutual coupling," *IEEE Trans. Antennas Propag.*, Vol. 54, No. 7, 1991–1996, Jul. 2006.
13. Jensen, M. A. and Y. Rahmat-Samii, "EM interaction of handset antennas and a human in personal communications," *Proceedings of the IEEE*, Vol. 83, No. 1, 1106–1113, Jan. 1995.
14. Vaughan, R. G. and L. S. Neil, "Evaluation of antenna configurations for reduced power absorption in the head," *IEEE Transactions on Vehicular Technology*, Vol. 48, No. 5, 1371–1380, Sep. 1999.
15. Li, L. W., M. S. Leong, P. S. Kooi, and T. S. Yeo, "Specific absorption rates in human head due to handset antennas: A comparative study using FDTD method," *Journal of Electromagnetic Waves and Applications*, Vol. 14, No. 7, 987–1001, 2000.
16. Kang, X. K., L. W. Li, M. S. Leong, and P. S. Kooi, "A method of moments study of SAR inside spheroidal human head and current distribution along handset wire antennas," *Journal of Electromagnetic Waves and Applications*, Vol. 15, No. 1, 61–76, 2001.
17. Kouveliotis, N. K., P. J. Papakanellos, E. D. Nanou, N. I. Sakka, V. S. G. Tsiafakis, and C. N. Capsalis, "Correlation between SAR, SWR and distance of a mobile terminal antenna in front of an experimental validation," *Journal of Electromagnetic Waves and*

- Applications*, Vol. 17, No. 11, 1561–1581, 2003.
18. De Salles, A. A., C. R. Ferndadez, and M. Bonadiman, “FDTD simulations and measurements on planar antennas for mobile phones,” *Microwave and Optoelectronics Conference. IMOC 2003. Proceedings of the 2003 SBMO/IEEE MTT-S International*, Vol. 2, 1043–1048, Sep. 2003.
 19. Stavros, K. and K. S. Nikita, “Study of the coupling between human head and cellular phone helical antennas,” *IEEE Transactions on Electromagnetic Compatibility*, Vol. 46, No. 1, 62–70, Feb. 2004.
 20. Kouveliotis, N. K., S. C. Panagiotou, P. K. Varlamos, and C. N. Capsalis, “Theoretical approach of the interaction between a human model and a mobile handset helical antenna using numerical methods,” *Progress In Electromagnetics Research*, Vol. 65, 309–327, 2006.
 21. Klemm, M. and G. Troester, “EM energy absorption in the human body tissues due to UWB antennas,” *Progress In Electromagnetics Research*, Vol. 62, 261–280, 2006.
 22. Ebrahimi-Ganjeh, M. A. and A. R. Attari, “Interaction of dual band helical and PIFA handset antennas with human head and hand,” *Progress In Electromagnetics Research*, Vol. 77, 225–242, 2007.
 23. Kuo, L.-C., Y.-C. Kan, and H.-R. Chuang, “Analysis of a 900/1800-MHz dual-band gap loop antenna on a handset with proximate head and hand model,” *Journal of Electromagnetic Waves and Applications*, Vol. 21, No. 1, 107–122, 2007.
 24. Khodabakhshi, H. and A. Cheldavi, “Numerical analysis of human head interaction with PIFA antennas in cellular mobile communications,” *Progress In Electromagnetics Research B*, Vol. 22, 359–377, 2010.
 25. Priyadarshini, S. J., T. A. J. Mary, D. Sugumar, and C. S. Ravichandran, “Impact of SAR on human head modeling in Elevators using IFA,” *Applied Electromagnetics (APACE), 2010 IEEE Asia-Pacific Conference*, 1–5, Port Dickson, Nov. 9–11, 2010.
 26. Kusuma, A. H., A.-F. Sheta, I. Elshafiey, Z. Siddiqui, M. A. S. Alkanhal, S. Aldosari, S. A. Alshebeili, and S. F. Mahmoud, “A new low SAR antenna structure for wireless handset applications,” *Progress In Electromagnetics Research*, Vol. 112, 23–40, 2011.
 27. Chim, K.-C., K. C. L. Chan, and R. D. Murch, “Investigating the impact of smart antennas on SAR,” *IEEE Trans. Antennas*

- Propag.*, Vol. 52, No. 5, 1370–1374, May 2004.
28. Akimasa, H., S. Mitsuzono, and T. Shiozawa, “Feasibility study of adaptive nulling on handset for 4G mobile communications,” *IEEE Antennas and Wireless Propagation Letters*, Vol. 3, 120–122, 2004.
 29. Chen, Q., Y. Komukai, and K. Sawaya, “SAR investigation of array antennas for mobile handsets,” *IEICE Trans. Commun.*, Vol. E90-B, No. 6, 1354–1356, Jun. 2007.
 30. Chen, H.-Y. and H. Yang, “SAR affected by shapes and electrical properties of the human head exposed to the cellular phone,” *Microwave and Optical Technology Letters*, Vol. 42, No. 1, 1–4, Jul. 2004.
 31. Yoshida, K., A. Hirata, Z. Kawasaki, and T. Shiozawa, “Human head modeling for handset antenna design at 5 GHz band,” *Journal of Electromagnetic Waves and Applications*, Vol. 19, No. 3, 401–411, 2005.
 32. Mahmoud, K. R., M. El-Adawy, S. M. M. Ibrahim, R. Bansal, and S. H. Zainud-Deen, “Investigating the interaction between a human head and a smart handset for 4G mobile communication systems,” *Progress In Electromagnetics Research C*, Vol. 2, 169–188, 2008.
 33. Sanchez-Montero, R., S. Salcedo-Sanz, J. A. Portilla-Figueras, and R. Langley, “Hybrid pifa-patch antenna optimized by evolutionary programming,” *Progress In Electromagnetics Research*, Vol. 108, 221–234, 2010.
 34. Kennedy, J. and R. Eberhart, “Particle swarm optimization,” *IEEE International Conference on Neural Networks*, Vol. 4, 1942–1948, Perth, Australia, 1995.
 35. Nelder, J. A. and R. Mead, “A simplex method for function minimization,” *Computer Journal*, Vol. 7, 308–313, 1965.
 36. Atef, E. and V. Demir, *The Finite Difference Time Domain Method for Electromagnetics: With MATLAB Simulations*, Har/Cdr Edition, SciTech Publishing, 2009.
 37. CST Microwave Studio Suite 2011 User’s Manual, www.cst.com.
 38. Gabriel, S., R. W. Lau, and C. Gabriel, “The dielectric properties of biological tissues: II. Measurements in the frequency range 10 Hz to 20 GHz,” *Phys. Med. Biol.*, Vol. 41, 2251–2269, 1996.